Defect imaging for plate-like structures using diffuse field

AUTHOR(S):

Hayashi, Takahiro

CITATION:

Hayashi, Takahiro. Defect imaging for plate-like structures using diffuse field. The Journal of the Acoustical Society of America 2018, 143(4): EL260.

ISSUE DATE:

2018-04

URL:

http://hdl.handle.net/2433/230946

Defect imaging for plate-like structures using diffuse field

Takahiro Hayashi

Citation: The Journal of the Acoustical Society of America **143**, EL260 (2018); doi: 10.1121/1.5030915
View online: https://doi.org/10.1121/1.5030915
View Table of Contents: http://asa.scitation.org/toc/jas/143/4
Published by the Acoustical Society of America

Takahiro Hayashi: JASA Express Letters https://doi.org/10.1121/1.5030915 Published Online 12 April 2018

Defect imaging for plate-like structures using diffuse field

Takahiro Hayashi
Graduate School of Engineering, Kyoto University, Kyoto, 615-8540, Japan
hayashi@kuaero.kyoto-u.ac.jp

Abstract: Defect imaging utilizing a scanning laser source (SLS) technique produces images of defects in a plate-like structure, as well as spurious images occurring because of resonances and reverberations within the specimen. This study developed defect imaging by the SLS using diffuse field concepts to reduce the intensity of spurious images, by which the energy of flexural waves excited by laser can be estimated. The experimental results in the different frequency bandwidths of excitation waves and in specimens with different attenuation proved that clearer images of defects are obtained in broadband excitation using a chirp wave and in specimens with low attenuation, which produce diffuse fields easily.

[NV]
Date Received: October 13, 2017 **Date Accepted:** March 25, 2018

1. Introduction

Elastic waves and ultrasonic waves are widely used in the non-destructive evaluation (NDE) of materials. Measurement and signal processing techniques using elastic waves and ultrasonic waves such as C-scans, tomography, the synthetic aperture focusing technique (SAFT), and phased arrays provide images of the inner conditions of a material, and have become invaluable in industrial fields. This is because these imaging techniques enable even non-expert inspection personnel to implement a quantitative NDE of materials.[1–4]

The most popular imaging technique for a plate structure is C-scans, in which images are acquired from the intensity of an ultrasonic wave transmitted through the plate. Originally, the ultrasonic wave was measured by through-transmission with ultrasonic transducers placed on both sides of the plate immerged in a water bath. Owing to high-performance air-coupled ultrasonic transducers, C-scan imaging for such plate-like structures has become feasible in air.[5,6]

Moreover, imaging techniques with guided waves that propagate along a plate have also been widely studied. For example, Hutchins *et al.*[7] visualized defects in a plate with tomography using Lamb waves. Sicard *et al.*[8,9] developed a SAFT with compensation for Lamb wave dispersions. Kundu *et al.* showed that defects stretching in the plate-thickness direction such as fiber breakage in fiber-reinforced composite plates, which are not detectable with conventional C-scan imaging, were visualized using an L-scan in which Lamb waves were generated and detected by angle beam transducers.[10] These guided wave techniques have the great advantage of single-sided access. This is of practical use in the NDE of large products such as automobiles and aircraft. However, when a test plate has a small and complex shape, this method is not suitable for imaging because the many reflected waves are superposed with the wave used for investigation.

Therefore, the author of the current paper has been developing a defect-imaging technique for plate-like structures with complex geometries capable of taking measurements with single-sided access, using the characteristics of flexural vibration (A0 Lamb mode) excited by laser irradiation.[11–16] In this imaging technique, flexural vibration is generated in a plate by laser irradiation of the plate's surface, and the resulting flexural vibration is detected at a fixed position. One can observe variations in generation energy by rastering the elastic wave source of the laser beam, and by detecting numerous waveforms from all laser sources. Reference 16 explains that the generation energy reflects the apparent bending stiffness at the laser spot. When the laser spot and its vicinity have a smaller bending stiffness due to damage or wall-thinning, the flexural wave energy it generates is larger. When reflection objects such as notch-type defects exist in a plate, the interaction of evanescent modes from the laser source and the reflection objects induce energy enhancement. This phenomenon, discussed in Ref. 12, provides super-resolution imaging in plate-like structures in which

the resolution of defects exceeds the wavelength of flexural vibration. The author and his colleagues also explained that this imaging technique can be applied to the remote measurements of straight pipes and branch pipes using a laser Doppler vibrometer.[15] Moreover, this imaging technique provides stable measurements even with non-contact detection using a laser Doppler vibrometer because the receiving point is fixed. This leads to high-speed, non-contact imaging, as described in Ref. 14. Although the imaging technique using a scanning laser source (SLS) can be applied to plate-like structures, spurious images appear due to resonances and reverberations in the structure. Our previous researches[11–16] suggested that the averaging of images from multiple receivers or multiple frequencies is needed to reduce the spurious images.

However, defect-imaging with an SLS still produces large spurious images compared with other existing techniques such as C-scans, SAFT, and tomography. Therefore, in order to eliminate the spurious images due to reverberations and resonances in a plate and to provide clear defect images, this study proposes a new defect imaging technique using an SLS and a diffuse acoustic field that has an approximately uniform distribution of energy in the whole structure formed after multiple reflections. Furthermore, I experimentally confirm the validity of the new imaging technique.

2. Application of diffuse field concept to the defect imaging technique

The diffuse field concept was originally applied in the field of room acoustics, and then for analysis of acoustic emission signals. Egle[17,18] and Weaver[19,20] published theoretical and experimental studies on the diffuse field in solid media. Evans and Cawley[21] showed that the energy generated at a source can be predicted by calculating the energy transfer between thin plate structures, and the energy conversion between propagating modes using Statistical Energy Analysis (SEA). In these past studies, a diffuse field is well formed under the following conditions:

(i) Broadband waves are excited so that many resonant modes exist;
(ii) waves travel back and forth repeatedly in the enclosed structure with low attenuation; and
(iii) all resonant modes are generated at the same time, and the source is nondirectional.

Because narrowband waves consisting of a small number of resonant modes often form nodes and anti-nodes in the structure due to resonance, condition (i) is necessary. To create a diffuse field, an acoustic field with random distributions is necessary. In solid media with high attenuation and/or a large area, a random acoustic field is hardly formed due to small numbers of reflections from edges of the media. Moreover, an elastic wave source with intentional directivity like ultrasonic transducers also prevents a random field from forming. Therefore, conditions (ii) and (iii) are necessary. In past studies, because these conditions meet those of acoustic emission, the diffuse field concept has been used for analyzing the source energy of acoustic emission. It is recognized that the diffuse field concept can be applied to elastic wave measurements in our defect imaging technique by SLS, because flexural wave generation by a laser meets most of the requirements. Since condition (iii) holds all the time because of the point source of a laser beam, the relationships between diffuse field conditions (i) and (ii) and defect images are shown in the following experiments.

3. Results and discussions

3.1 Test plate

The test plate used in this study is an aluminum alloy plate with the dimensions 500 mm × 500 mm × 3 mm, with two notches stretching from the upper and lower edges at the centerline, dividing the plate into two substructures as shown in Fig. 1. These substructures are connected by a ligament of 60 mm through which the vibration energies exchange. On the back surface, artificial notches shaped like the letter "K" and a zigzag pattern, were engraved 2 mm wide and 1.5 mm deep, as shown in the figure. The laser beam was rastered over a 150 mm × 400 mm area in 2 mm increments, and the waveforms were detected with a piezoelectric transducer attached on the left substructure, as shown in the figure.

3.2 Defect imaging using narrowband burst wave

First, the results obtained for narrowband burst waves are shown. In our previous studies, narrowband burst waves were excited instead of pulse waves, to improve the signal-to-noise ratio (SNR) in the frequency domain, facilitating remote vibration detection with a laser Doppler vibrometer that has a much smaller SNR than contact transducers.[11–16] A detailed experimental setup can be found in Refs. 11–16. In this

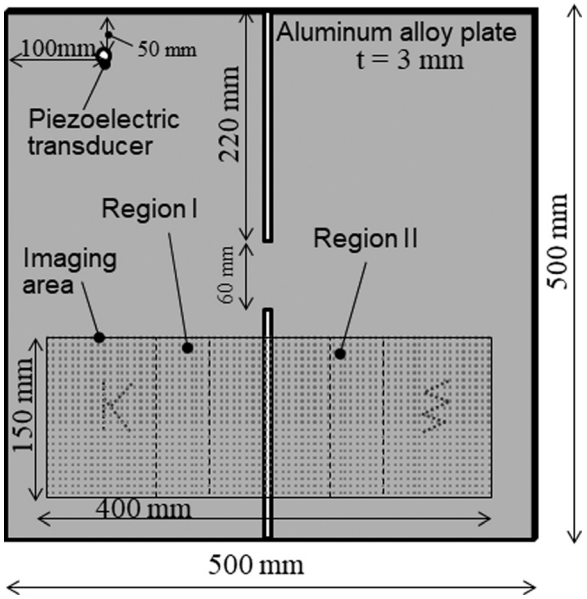

Fig. 1. Test plate used and positions of the receiving transducer and the laser irradiation area.

experiment, a narrowband elastic wave with a center frequency of 20 kHz was generated by the laser output that was modulated by rectangular signals with frequencies and durations of 20 kHz and 5 ms, respectively. The elastic waves generated by laser irradiation were detected by the piezoelectric transducer, and the signals were recorded 40 ms from the time of the laser output, on a personal computer, after undergoing 60 dB amplification through an analog to digital converter. In order to implement SEA of the numerous waveforms for all laser rastering positions, the waveforms were enveloped, the averages and the standard deviations of the envelope waveforms were calculated, and the distributions of the generation energy were created from the estimated values of generation energy for all laser positions.

The solid line in Fig. 2(a) shows an average of the envelope waveforms for all laser positions in region I of the left substructure, and the dashed lines denote the average ± standard deviation. Figure 2(b) shows an average and the average ± standard deviation for region II in the right substructure. The envelope waveforms were calculated by applying a high pass filter with a frequency of 1 kHz to the absolute values of waveforms. The modulation signals were activated and the laser beam was irradiated from 0 to 5 ms. In Fig. 2(a), the amplitude abruptly increased within approximately the first 1 ms, because the receiving transducer was in the same substructure as region I. Considering that the group velocity of the A0 mode at 20 kHz is approximately 1.4 m/ms for the plate, the receiving signal at 1 ms resulted in the mixture of waves traveling through various paths with multiple reflections and the waves traveling on the direct path. The fact that the interval maintained roughly constant amplitude after

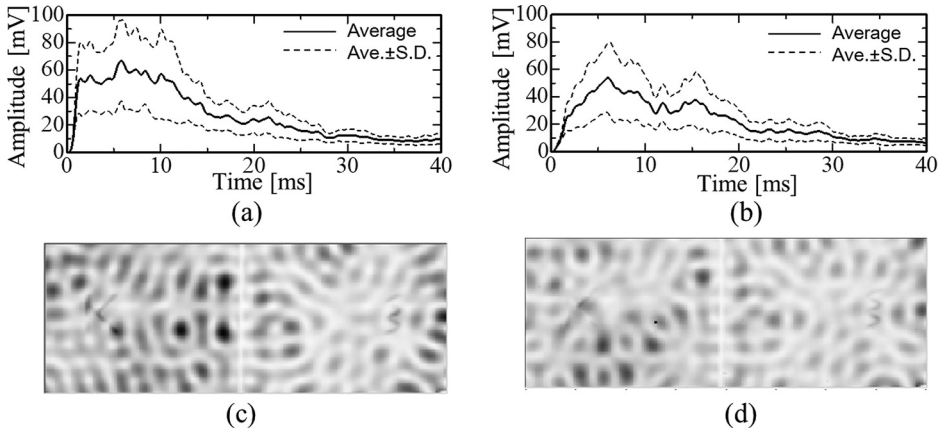

Fig. 2. Experimental results for a narrowband burst wave at 20 kHz. (a) Envelope wave at region I, (b) envelope wave at region II, (c) energy distribution in the time range from 0 to 20 ms, and (d) energy distribution in the time range from 20 to 40 ms.

the sudden increase shows that the input energy by laser irradiation was balanced by the energy reduction due to transfer to the right substructure, leakage to the air, and viscous damping in the plate. After approximately 6 ms, the envelope waveform gradually decreases. However, in Fig. 2(b), where the laser irradiation area and the receiving position are located in different substructures, the amplitude increased gradually from 0 ms because the waveforms were detected after traveling through the ligament. In both cases, the standard deviation is very large from 1 to 10 ms, meaning that the amplitudes are significantly different, depending on the positions of the laser source. After about 6 ms, the variations became gradually smaller because of the amplitude reduction. However, small variations remain even at 40 ms.

According to SEA for an ideal diffuse field, the integration of the square of an envelope waveform with respect to time is proportional to the vibration energy generated within the time range.[21] Here, Figs. 2(c) and 2(d) show the energy distributions obtained from the integration values of the envelope waveforms for all laser irradiation positions. The gray scale is normalized by the maximum value in the region; black and white denoting the maximum value and zero, respectively. In Figs. 2(c) and 2(d), the time ranges were set from 0 to 20 ms and 20 to 40 ms, respectively. The artificial defects of the letter "K" and the zigzag pattern are unclear due to the large quantity of spurious images in both Figs. 2(c) and 2(d). The spurious images correspond to the large variations in the envelope waveforms, as shown in Figs. 2(a) and 2(b). It has been demonstrated in our previous studies that the spurious images were caused by resonances in a structure.

3.3 Defect imaging using broadband chirp wave

In the experiment shown in Fig. 2, a narrowband tone-burst wave was used, in the same way as our previous studies. However, because it does not satisfy diffuse field condition (i) very well, a diffuse field was not well formed, and the amplitude variations due to the various laser positions remained for some time after the laser excitation. Therefore, an experimental result satisfying condition (i) is shown by generating broadband elastic waves. Although pulse excitation is useful to generate broadband elastic waves, a large pulse with an extremely high maximum energy is required to generate waves to the same extent as the burst wave generation. Because using high maximum energy may cause damage to the laser spot, a pulse wave is often less optimal than NDE. Here, a chirp wave was generated by applying a chirp modulation signal whose frequency linearly changed from 10 to 40 kHz, within the duration of 5 ms. Figures 3(a) and 3(b) are envelope waveforms for regions I and II, respectively, as in Figs. 2(a) and 2(b), with solid lines and dashed lines denoting the average and the average ± standard deviation, respectively. In both figures, the average curves increase up to about 60 mV, which is the same level as the burst wave generation shown in Figs. 2(a) and 2(b). In Fig. 3(a), the amplitude increases abruptly within approximately the first 1 ms, and then the amplitude roughly maintains the maximum value until about 5 ms, while in Fig. 3(b), the average amplitude increases gradually. These tendencies in the average amplitude for the chirp excitation are also similar to those of the burst excitation shown in Figs. 2(a) and 2(b). However, the standard deviations, representing the amplitude variations depending on the laser positions, are significantly

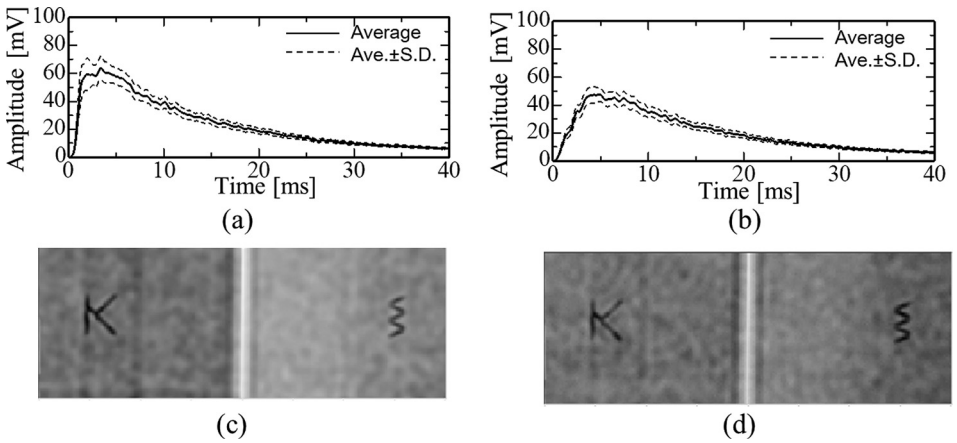

Fig. 3. Experimental results for a chirp wave from 10 to 40 kHz. (a) Envelope wave at region I, (b) envelope wave at region II, (c) energy distribution in the time range from 0 to 20 ms, and (d) energy distribution in the time range from 20 to 40 ms.

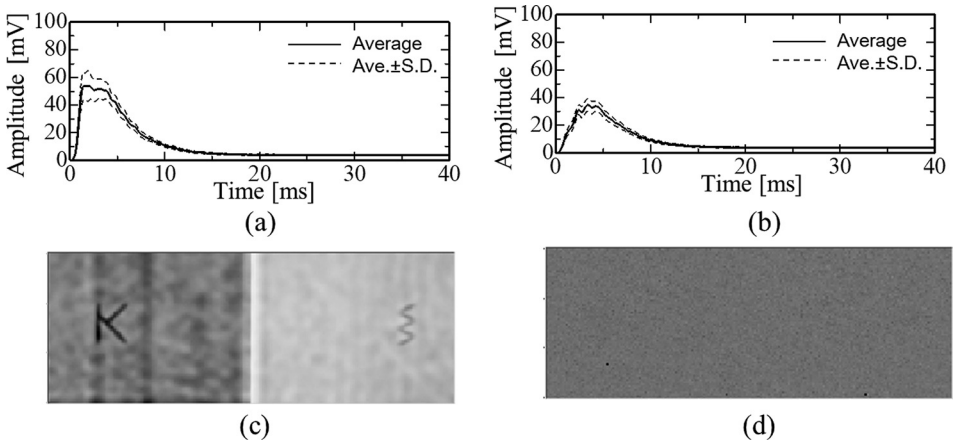

Fig. 4. Experimental results for a high-attenuated plate. A chirp wave ranging from 10 to 40 kHz was used. (a) Envelope wave at region I, (b) envelope wave at region II, (c) energy distribution in the time range from 0 to 20 ms, and (d) energy distribution in the time range from 20 to 40 ms.

smaller than those in Figs. 2(a) and 2(b). These results indicate that the use of broadband waves is effective in forming a diffuse field.

The energy distributions obtained from these waveforms are shown in Figs. 3(c) and 3(d), where the time range is 0–20 and 20–40 ms, respectively. In both figures, spurious images are significantly reduced and defect images clearly appear. These results correspond to the results in Figs. 3(a) and 3(b), where the standard deviations become smaller than those in Figs. 2(a) and 2(b). Comparing Fig. 3(c) with Fig. 3(d), it can be seen that Fig. 3(d) has a more uniform distribution between the left and right substructures. This is because the vibration energies in the left and right substructures approximate the same energy levels of ideal diffuse fields with the elapse of time.

3.4 Defect imaging for a plate with high attenuation

To test diffuse field condition (ii), experiments were conducted using a test plate with higher attenuation. Adhesive tapes that were 18 mm wide were attached around all sides of the test plate, so that reflections from the edges could be suppressed.

Figures 4(a) and 4(b) are averaged envelope waveforms (solid lines) and the averages ± standard deviations (dashed lines) for regions I and II, respectively, as shown in Figs. 2(a) and 2(b) and Figs. 3(a) and 3(b). In both regions, the averaged waveforms become approximately 10–20 mV smaller than those in Figs. 2(a) and 2(b) or Figs. 3(a) and 3(b). This shows that the adhesive tape surrounding the plate edge reduces vibration energy in the plate. Figures 4(c) and 4(d) are vibration energy distributions, similar to Figs. 2(c) and 2(d) and Figs. 3(c) and 3(d). In Fig. 4(c), for the time range of 0–20 ms, the energies in the left and right substructures were significantly different, even though defect images were appropriately obtained. This result, as seen in Fig. 3(c), shows that the energies in the left and right substructures did not rise to the same level during the time range. However, Fig. 4(d), which shows the time range of 20–40 ms, did not create defect images at all, which means that the vibration energies dissipated before the energies in both substructures became uniform, due to the high attenuation of the structure.

The experimental results detailed above show that clearer defect images with fewer spurious images can be obtained using a diffuse field in the structure. However, no images can be created from waveforms that are too small, even though wave fields generated by lasers approach ideal diffuse fields with the elapse of time. Therefore, an appropriate time range must be chosen, depending on the plate structure to be inspected.

Acknowledgment

This work was supported by JSPS KAKENHI Grant No. 17H02052.

References and links

[1]B. Grohs, O. A. Barbian, W. Kappes, H. Paul, R. Licht, and F. W. Hoh, "Characterization of flaw location, shape, and dimensions with the ALOK system," Mater. Eval. **40**, 84–89 (1982).
[2]D. W. Prine, "Synthetic aperture ultrasonic imaging," Proc. Eng. Appl. Holography Symp. 287–288 (1972).
[3]S. R. Doctor, T. E. Hall, and L. D. Reid, "SAFT—The evolution of a signal processing technology for ultrasonic testing," NDT Int. **19**, 163–167 (1986).

[4]B. W. Drinkwater and P. D. Wilcox, "Ultrasonic arrays for non-destructive evaluation: A review," NDT&E Int. **39**, 525–541 (2006).
[5]D. W. Schindel and D. A. Hutchins, "Through-thickness characterization of solids by wideband air-coupled ultrasound," Ultrasonics **33**, 11–17 (1995).
[6]D. E. Chimenti, "Review of air-coupled ultrasonic materials characterization," Ultrasonics **54**, 1804–1816 (2014).
[7]D. A. Hutchins, D. P. Jansen, and C. Edwards, "Lamb-wave tomography using non-contact transduction," Ultrasonics **31**, 97–103 (1993).
[8]R. Sicard, J. Goyette, and D. Zellouf, "A SAFT algorithm for lamb wave imaging of isotropic plate-like structures," Ultrasonics **39**, 487–494 (2002).
[9]R. Sicard, A. Chahbaz, and J. Goyette, "Guided lamb waves and L-SAFT processing technique for enhanced detection and imaging of corrosion defects in plates with small depth-to-wavelength ratio," IEEE Trans. Ultrason. Ferroelectr. Freq. Control. **51**, 1287–1297 (2004).
[10]T. Kundu, K. Maslov, P. Karpur, T. E. Matikas, and P. D. Nicolaou, "A Lamb wave scanning approach for the mapping of defects in [0/90] titanium matrix composites," Ultrasonics **34**, 43–49 (1996).
[11]T. Hayashi, "Imaging defects in a plate with complex geometries," Appl. Phys. Lett. **108**, 081901 (2016).
[12]T. Hayashi and M. Fukuyama, "Vibration energy analysis of a plate for defect imaging with a scanning laser source technique," J. Acoust. Soc. Am. **140**, 2427–2436 (2016).
[13]T. Hayashi and K. Ishihara, "Generation of narrowband elastic waves with a fiber laser and its application to the imaging of defects in a plate," Ultrasonics **77**, 47–53 (2017).
[14]T. Hayashi, "High-speed non-contact defect imaging for a plate-like structure," NDT&E Int. **85**, 53–62 (2017).
[15]T. Hayashi, "Non-contact imaging of pipe thinning using elastic guided waves generated and detected by lasers," Int. J. Press. Vessel. Pip. **153**, 26–31 (2017).
[16]T. Hayashi and S. Nakao, "Energy analyses for the imaging technique of bonded regions and delaminations in a thin plate," Mater. Trans. **58**, 1264–1273 (2017).
[17]D. M. Egle, "A stochastic model for transient acoustic emission signals," J. Acoust. Soc. Am. **65**, 1198–1203 (1979).
[18]D. M. Egle, "Diffuse wave fields in solid media," J. Acoust. Soc. Am. **70**, 476–480 (1981).
[19]R. L. Weaver, "On diffuse waves in solid media," J. Acoust. Soc. Am. **71**, 1608–1609 (1982).
[20]R. L. Weaver, "Diffuse waves in finite plates," J. Sound Vib. **94**, 319–335 (1984).
[21]M. J. Evans and P. Cawley, "Measurement and prediction of diffuse fields in structures," J. Acoust. Soc. Am. **106**, 3348–3361 (1999).